Journal of
Ceramic Science
and Technology

J. Ceram. Sci. Technol., **09** [2] 155-162 (2018)
DOI: 10.4416/JCST2017-0090
available online at: http://www.ceramic-science.com

Enhanced Electrochemical Performance of Cu-Doped $La_2NiO_{4+\delta}$ Cathode for Solid Oxide Fuel Cells

H. Chen[1, 2], X. Li[2], X. Du[2], H. Xie[2], L. Zhao[*3], Y. Ling[*1, 2]

[1]Key Laboratory of Coal-based CO_2 Capture and Geological Storage, China University of Mining and Technology, Xuzhou 221116, P.R. China
[2]School of Materials Science and Engineering, China University of Mining and Technology, Xuzhou 221116, P.R. China
[3]Department of Material Science and Chemistry, China University of Geosciences, Wuhan 430074, P.R. China

received November 15, 2017; received in revised form December 21, 2017; accepted January 10, 2018

Abstract

To illustrate the effect of Cu-doping in Ruddlesden-Popper-type $La_2NiO_{4+\delta}$ oxides, the crystal structure, interstitial oxygen formation, electrical conductivity, catalytic activity and chromium tolerance of $La_2NiO_{4+\delta}$(LNO)and $La_2Ni_{0.9}Cu_{0.1}O_{4+\delta}$(LNCO) are analyzed. XRD Rietveld and HT-TEM results confirm that both can be identified as Ruddlesden-Popper-type structures with tetragonal symmetry. Compared with non-doped LNO, LNCO has less interstitial oxygen, and its electrical conductivity decreases owing to the reduction of the carrier concentration. The effects on electrode performance are analyzed using symmetric cells, and interface polarization resistance at 800 °C is reduced from 2.20 Ωcm^2 to 0.54 Ωcm^2 after Cu-doping. Experimental results together with the excellent chromium tolerance confirmed by HT-XRD results demonstrate that Cu-doped LNO can work as a promising chromium-tolerant cathode.

Keywords: Ruddlesden-Popper-type oxide, interstitial oxygen, interface polarization resistance, chromium-tolerant cathode

I. Introduction

Ruddlesden-Popper (RP) oxides, $A_{n+1}B_nO_{3n+1}$, consisting of alternate n-perovskite (ABO_3)-layers and AO rock salt layers along the c-axis, can exhibit large oxygen non-stoichiometry, intrinsic mixed ionic-electronic conductivity, and excellent catalytic activity as typical high-performance cathode materials [1–5]. One-perovskite-layer oxide, $La_2NiO_{4+\delta}$ (LNO), has large interstitial oxygen, providing excellent oxygen diffusivity with low activation energy [5,6]. Compared to Co-containing cathode materials such as $Ba_{1-x}Sr_xCo_{1-y}Fe_yO_{3-\delta}$ and $Ln_{1-x}Sr_xCo_{1-y}Fe_yO_{3-\delta}$, it also exhibits a low thermal expansion coefficient of 12.6×10^{-6} K^{-1}, good structural compatibility and chemical stability with IT electrolytes [7]. However, pure LNO shows large-area specific resistance of 15.27 Ωcm^2 at 700 °C for the symmetrical cell of LNO/YSZ/LNO[8]. Low cell performance (91 mWcm^{-2} at 700 °C) with LSGM electrolyte was observed, indicating that LNO-based cathode performance should be further improved based on optimization of the cathode composition and microstructures [9]. Furthermore, high oxygen flux in LNO can generally be observed owing to high interstitial oxygen concentration, but it also decreases defect mobility and causes the change in the electronic configuration[10].

One effective way is that appropriate acceptor doping on the La-site with alkaline earths such as Sr and Ca can improve the electronic conductivity in p-type conductor LNO owing to the extra generating electron holes (Ni_{Ni}) by the charge compensation [11]. However, the substitution of La by alkaline earths causes the reduction of interstitial oxygen concentration, resulting in the ionic conductivity of LNO[12,13]. Furthermore, chromium deposition is easily generated on alkaline-earth-containing cathode materials, resulting in a rapid degradation of cell performance [14–17]. Another strategy has been proposed based on doping of a slight amount in the Ni-site with other transition metals. Compared to undoped LNO, $La_2Ni_{0.9}Cu_{0.1}O_{4+\delta}$ (LNCO) has less interstitial oxygen [10], but much higher oxygen diffusion with fast surface exchange rate was observed at intermediate temperatures for Cu-doping. That is because Cu-doping can shorten the Ni(Cu)-O(equatorial) bond in the Ni(Cu)O_6 octahedron and mitigate the rotation of the Ni(Cu)O_6 octahedron owing to the Jahn-Teller effect [18]. Moreover, Cu-doping in LNO could increase the sintering activity, which helps achieve an excellent cathode-electrolyte interface, and is beneficial to oxygen-ion transport through this interface [19,20]. In this work, Cu was selected as a dopant in LNO in order to improve sinterability and electrode performance. LNO and LNCO are prepared, and then the effects of Cu on the crystal structure, interstitial

* Corresponding author: lyhyy@mail.ustc.edu.cn
co-corresponding author: zhaoling@mail.ustc.edu.cn

oxygen, electrical conductivity and catalytic activity, and chromium tolerance are comparatively investigated and evaluated.

II. Experimental

LNO and LNCO were prepared in a citric acid-EDTA process as described in our previous work [21]. X-ray photoelectron spectroscopy (XPS, $h\upsilon = 1486.6$ eV) was applied to analyze the valence of the composition elements. Electrical conductivity was measured with an H.P. multimeter with the standard d.c. four-probe technique at 400 – 800 °C in air. The chemical compatibility of LNO and LNCO with Cr_2O_3, mixed in a weight ratio of 1:1, was investigated with high-temperature XRD from 500 °C to 900 °C.

To comparatively evaluate the electrochemical activity at the two LNO and LNCO cathodes on the GDC electrolyte, the configuration of cathode/GDC (~1 mm)/cathode (~30 μm) was fabricated to test symmetrical electrochemical cells as previously described [22]. AC impedance spectroscopy (Chi604c, Shanghai Chenhua) was used to analyze symmetrical electrochemical cells from 500 to 700 °C.

III. Result and Discussion

Fig. 1 presents XRD patterns of LNO and LNCO powders sintered at 1100 °C for 3 h in air. Both as-prepared oxides were identified as Ruddlesden-Popper-type structures, and agreed well with the reported data[6]. GSAS software for Rietveld refinements was used to further confirm two XRD patterns, and the refinement parameters are presented in Table 1. It can be observed that LNO and LNCO oxides exhibited the tetragonal structure with the space group of I4/mmm(139), indicating the experimental and calculated results present excellent consistency. Although Cu-doping in LNO cannot change the symmetry of the Ruddlesden-Popper-type lattice, the lattice parameter parallel to the rock salt layer after Cu-doping slightly decreases because of the shorter Ni(Cu)-O(equatorial) bond in the $Ni(Cu)O_6$ octahedron [19]. The rock salt and octahedron structure jointly cause a small increase of the lattice parameter perpendicular to the rock salt layer, which is in good agreement with Nakamura's study [10]. Moreover, HT-TEM images of LNO and LNCO corresponding to the lattice spacing of 0.3688 nm(101) and 0.3678 nm(101) are given in Fig. 2, respectively, and the results are consistent with those obtained with XRD analysis.

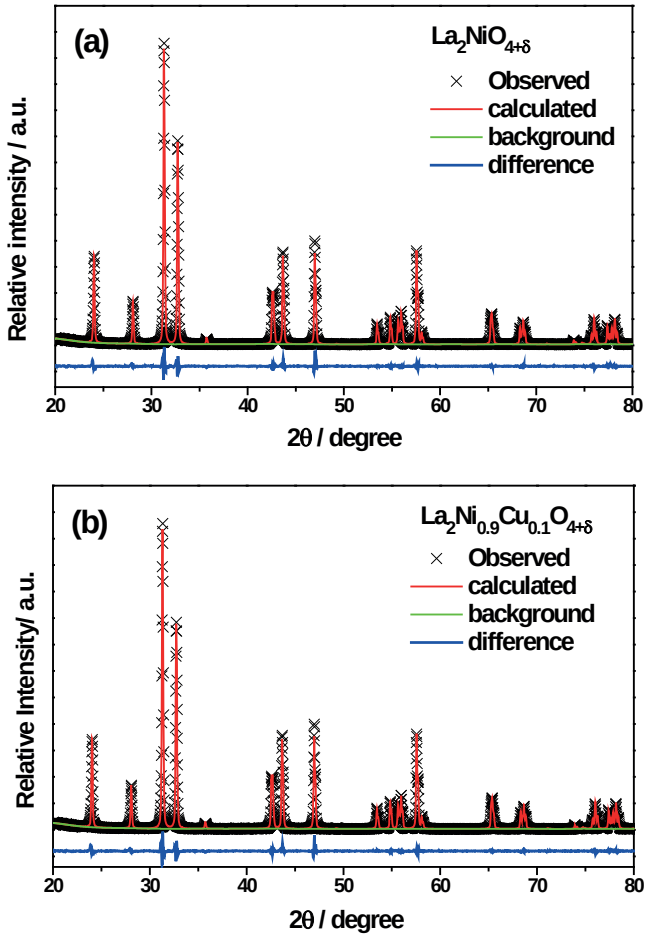

Fig. 1: XRD Rietveld refinement of as-prepared LNO (a) and LNCO (b) calcined at 1100 °C for 3 h in air.

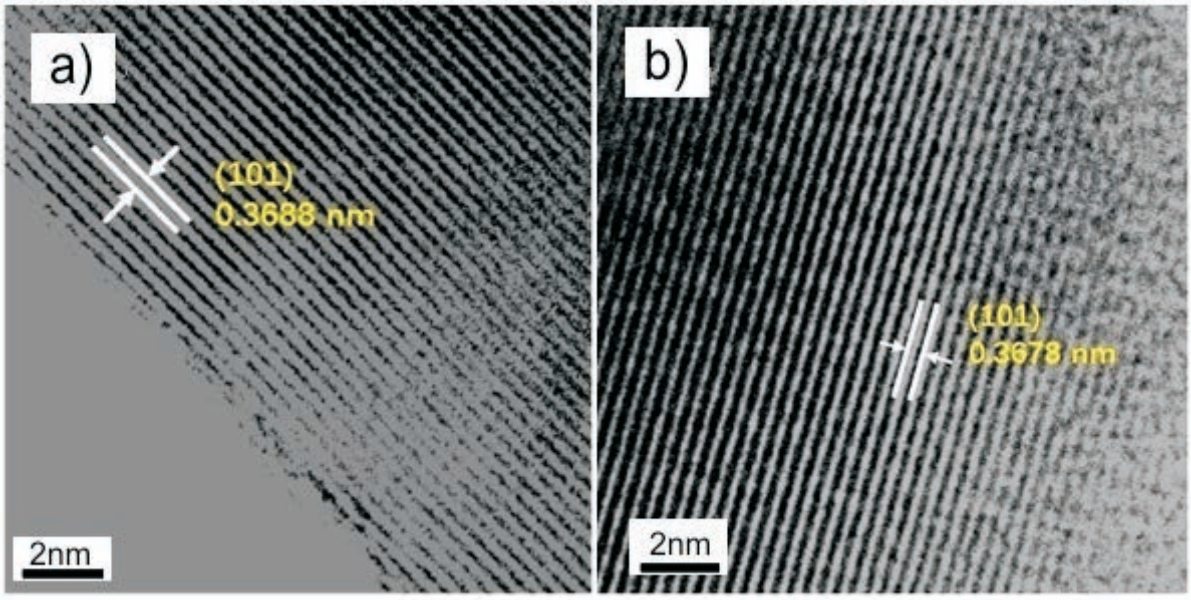

Fig. 2: HT-TEM images of LNO (a) and LNCO (b).

Table 1: Refinement parameters derived from XRD patterns.

Composition	wR_p(%)	R_p(%)	χ^2	a(Å)	c(Å)	v(nm^3)
$La_2NiO_{4+\delta}$	8.31	5.93	0.8475	3.8567(4)	12.6654(2)	188.39
$La_2Ni_{0.9}Cu_{0.1}O_{4+\delta}$	8.52	6.07	0.8037	3.8553(8)	12.7115(5)	188.94

To estimate the concentration of the interstitial oxygen, XPS was used to analyze the different chemical states in LNO and LNCO, where all these elemental valences were analyzed with the method of Shirley-type background subtraction, and every background function of elements was fitted by 20 % Lorenz and 80 % Gaussian. Fig. 3(a-c) and Fig. 4 (a-d) show the XPS spectroscopies of as-prepared LNO and LNCO samples, respectively. The La3d core level XPS spectra of LNO are shown in Fig. 3(a), where three binding energies at 833.1, 834.5 and 837.7 eV assigned as La^{3+} 3d 5/2, and three binding energies at 850.3, 851.3 and 854.2 eV assigned as La^{3+} 3d 3/2 are observed, which are very close to the similar compounds with La^{3+} in LNO [23]. Fig. 3(b) shows the Ni2p core level XPS spectra of LNO, wherethe main chemical states of Ni are +2 and +3. Ni^{2+} (2p 1/2), and Ni^{2+} (2p 3/2) peaks are found at 854.5 eV and 851.2 eV, respectively, while Ni^{3+} (2p 1/2) and Ni^{3+} (2p 3/2) peaks occur at 864.1 eV and 849.9 eV, in which the ratio of Ni^{2+}/ Ni^{3+} as calculated is about 58.7:41.3. The O1s core level XPS spectra of LNO are given in Fig. 3(c) and the binding energies are 531 and 528.5 eV. According to the charge neutrality in LNO, the interstitial oxygen concentration can be calculated to be 0.2065. It is observed that the interstitial oxygen concentration measured with XPS is a little higher than that measured with high-temperature TG (about 0.12 at 600 °C [10]), that is because the samples for XPS measurements were analyzed at room temperature, and the reference value by high-temperature TG was given at 600 °C. The lower the temperature, the higher the interstitial oxygen concentration should be. Accordingly, the La3d, Ni2p, Cu2p and O1s core level XPS spectrum of LNCO are presented in Fig. 4(a-d), respectively. Cu-doping in LNO presents no obvious change of the chemical state of Ni. However, the calculated ratio of Ni^{3+} is reduced to only 33 %, indicating that the interstitial oxygen concentration is 0.165, which is similar to findings that Cu-doping has less interstitial oxygen[1]. Fig. 4(c) presents the Cu2p core level XPS spectra wherethe main chemical state of Cu is +2 and the binding energies are 933.6 eV and 942.2 eV, indicating no monovalent Cu exists. It can be inferred that the Cu incorporation in $Ni(Cu)O_6$ octahedron structure restricts oxygen insertion into the rock salt layer owing to much stronger distortion in $Cu^{2+}O_6$ (d9 state) than in $Ni^{2+}O_6$ (d8 state), and thus LNCO has a smaller oxygen content than LNO [10].

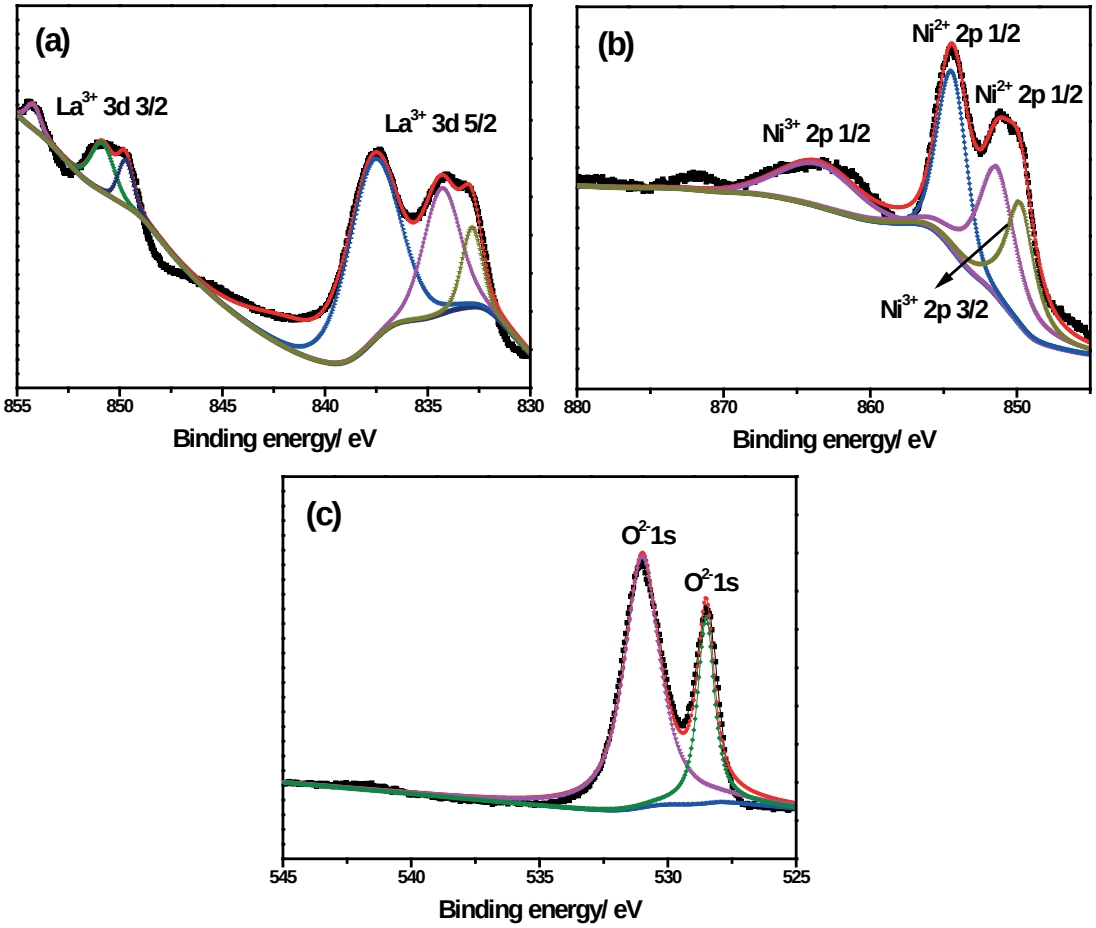

Fig. 3: XPS spectroscopy of La3d (a), Ni2p (b), and O1s (c) of LNO.

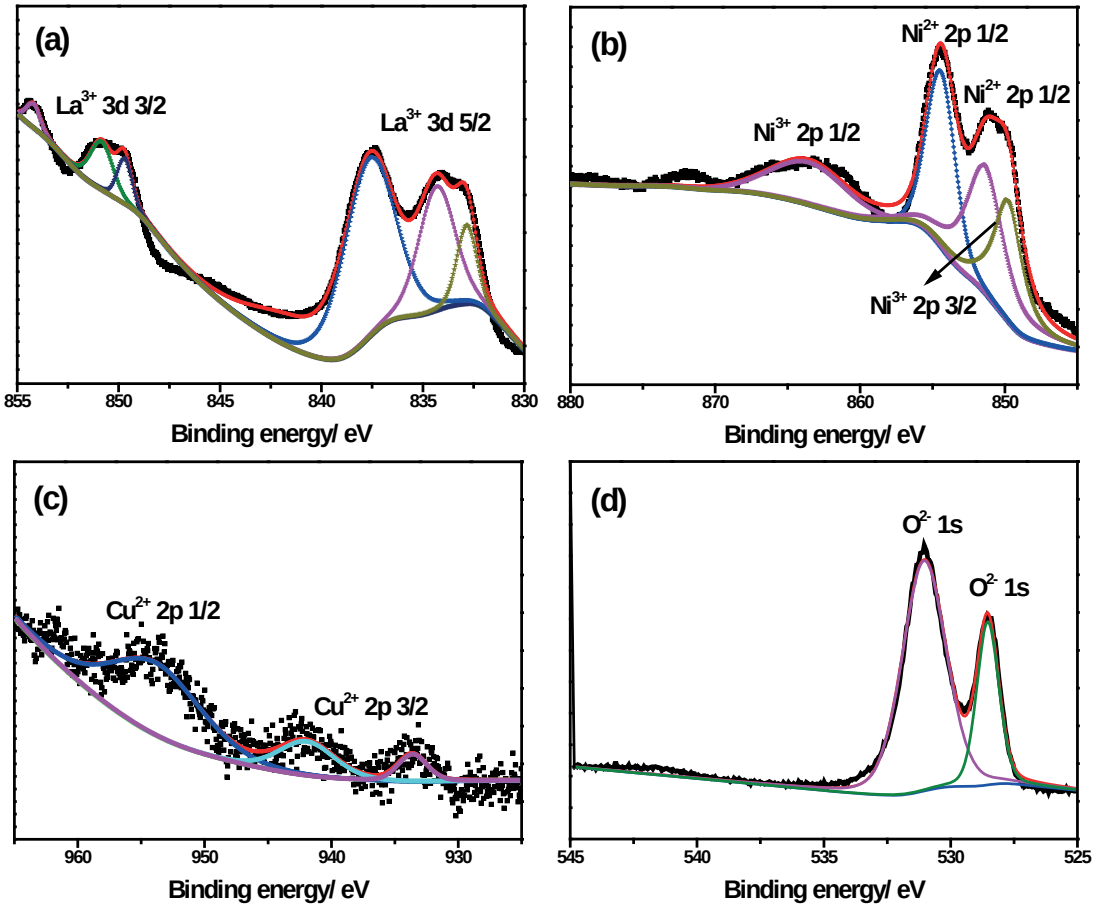

Fig. 4: XPS spectroscopy of La3d (a), Ni2p (b), Cu2p (c) and O1s (d) of LNCO.

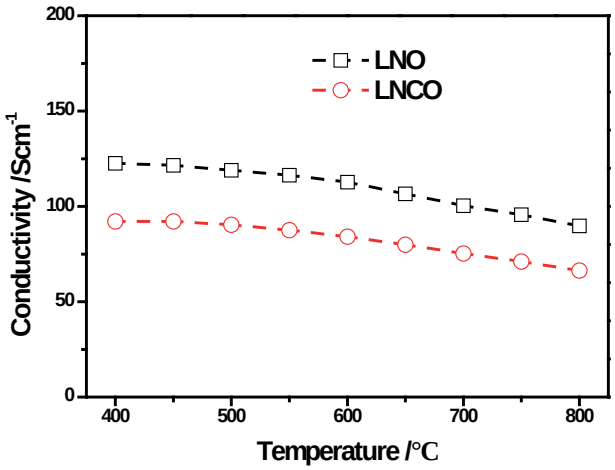

Fig. 5: Temperature dependence of the conductivity for LNO and LNCO samples.

The electrical properties in LNO-based oxides greatly depend on the interstitial oxygen and holes for electrochemical devices. Meanwhile, the oxygen incorporation in LNO-based oxides can also result in the production of the interstitial oxygen and holes as follows:

$$\frac{1}{2}O_2 + V_i^{\times} \leftrightarrow O_i'' + 2h^{\cdot} \qquad (1)$$

Fig. 5 shows the electrical conductivity curves of LNO and LNCO samples in air, respectively. The electrical conductivity of LNO gently decreases as the temperature increases, and the maximum value of 122.6 S cm^{-1} is observed at about 400 °C, suggesting that thermally deactivated metal-like band conduction at high temperatures [24]. After Cu-doping in LNO, the electrical conductivity decreases, and the maximum value of 92.2 Scm^{-1} is observed at about 400 °C. Generally, the electrical conductivity mainly depends on the carrier concentration and mobility, and can be expressed by

$$\sigma_p = N_p \mu_p P \qquad (2)$$

where N_p, μ_p and P are the volume concentration, the mobility and the concentration of carriers, respectively. Therefore, the difference in the electrical conductivity in LNO and LNCO is mainly caused by the different carrier concentration, which depends on the amount of interstitial oxygen in accordance with the above results [25, 26].

In LNO-based oxides, both oxygen vacancy and interstitial oxygen are active oxygen point defects for the electrochemical properties, and there is an exchange reaction between the oxygen vacancy and interstitial oxygen:

$$O_O^{\times} + V_i^{\times} \leftrightarrow V_O^{\cdot\cdot} + O_i'' \qquad (3)$$

The balance of oxygen vacancy and interstitial oxygen determine the oxygen transport properties like oxygen surface exchange and bulk transport, which greatly affects the electrochemical properties [27]. To understand the effects of Cu-doping in LNO on electrode performance, symmetric cells with LNO and LNCO electrode were evaluated based on AC impedance at the temperature range of 800 – 550 °C as shown in Fig. 6. The value of the ohmic resistance (Ro) is the first intercept of the Z'axis at high frequencies, while the polarization resistance (Rp) is the difference between the first and last intercept of the Z'axis at low frequencies, where Ro and Rp generally

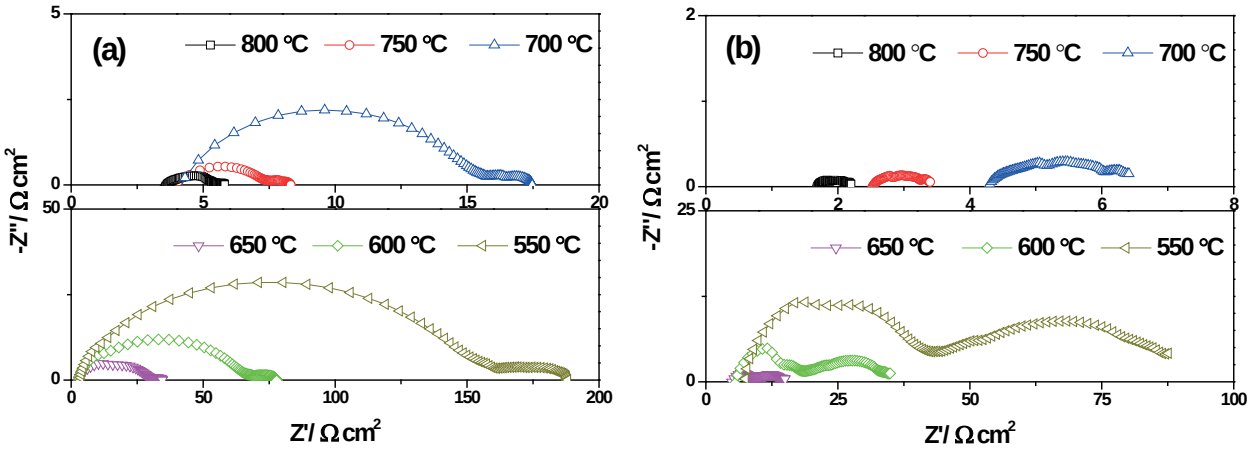

Fig. 6: The AC impendence of the symmetric cells with LNO (a) and LNCO (b) electrodes from 800 °C to 550 °C.

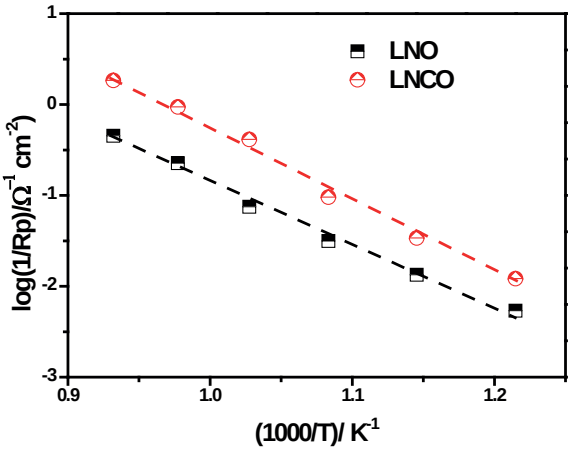

Fig. 7: The apparent activation energy of interfacial polarization resistances for LNO and LNCO electrodes.

increase gradually with decreasing temperature [28]. It can be observed in Fig. 6(a) that Rp for LNO significantly increased from 2.20 Ωcm^2 at 800 °C to 185.48 Ωcm^2 at 550 °C, respectively. After Cu-doping in LNO, Rp is reduced to 0.54 Ωcm^2 at 800 °C and 82.14 Ωcm^2 at 550 °C as shown in Fig. 6(b), respectively. The activation energy (Ea) for Rp of LNO is 141.75 kJ mol^{-1} as shown in Fig. 7, and LNCO has a low Ea (116.79 kJ mol^{-1}), which has a greater advantage in low temperature compared with $La_{0.8}Sr_{0.2}Co_{0.8}Fe_{0.2}O_{3-\delta}$ (Ea = 202 kJ mol^{-1}) and $La_{0.8}Sr_{0.2}CoO_{3-\delta}$, (Ea = 164 kJ mol^{-1}) [29].

Now we briefly evaluate the contribution to the electrochemical properties of LNO-based oxides on the carrier concentration, interstitial oxygen and oxygen vacancy. From above electrical conductivity results, the more the carrier concentration, the higher the electrical conductivity. However, the electrical conductivity is not the most important factor for the electrochemical properties while the electrical conductivity is around 100 Scm^{-1}, for example, $Ba_{0.5}Sr_{0.5}Co_{0.8}Fe_{0.2}O_{3-\delta}$ [30]. A. Aguadero et al. [31] reported that the polarization resistance of $La_2Ni_{1-x}Cu_xO_{4+\delta}$ on LSGM electrolyte decreases with Cu content, indicating that high interstitial oxygen concentration does not necessarily result in high catalytic activity. For Sr doping in LNO-based oxides, the oxygen non-stoichiometry can also greatly affect the conduction mechanism, the electronic state and the electrochemical properties [12, 32, 33]. Importantly, oxygen defect species in two-perovskite-layer oxide, $Sr_3Fe_2O_{7-\delta}$, are oxygen vacancies located in the apical O1 and equatorial O3 lattices, and $Sr_3Fe_2O_{7-\delta}$ still exhibited excellent mixed ionic and electronic transport properties [34, 35]. Accordingly, the cathode microstructure and the excellent matching between the electrode and the electrolyte material can also greatly affect the electrochemical properties.

To analyze the effect of the chromium tolerance of LNO and LNCO, Fig. 8 shows the high-temperature XRD

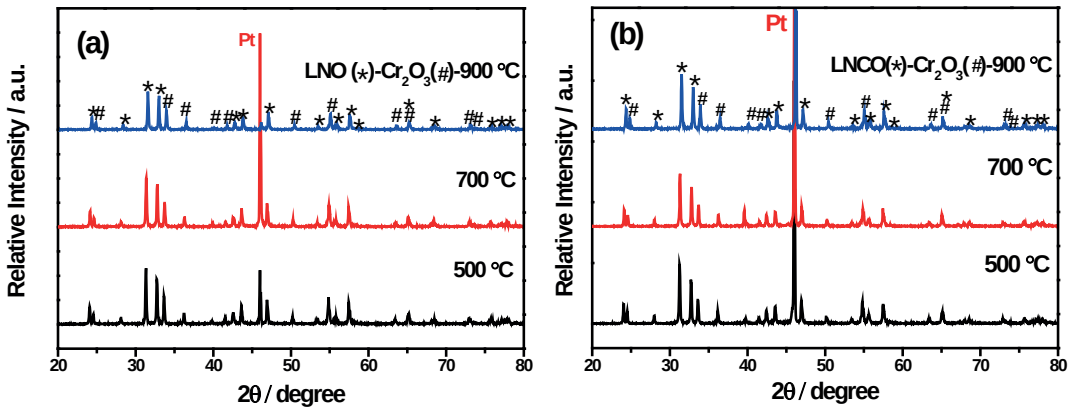

Fig. 8: Chemical compatibility of LNO (a) and LNCO (b) with Cr_2O_3 measured by means of high-temperature XRD from 500 °C to 900 °C.

results of LNO and LNCO with Cr_2O_3 mixture (the weight ratio of 1:1), respectively, because Cr is uniformly distributed in the interior of the electrode with Cr_2O_3. From 500 °C up to 900 °C, both LNO and LNCO with a K_2NiF_4-type structure and Cr_2O_3 with a corundum type structure can only be observed, and no new peaks are produced, indicating a relatively high chromium tolerance of LNO and LNCO below 900 °C. All in all, there is no chemical reaction between Cr_2O_3 and the electrodes. The experimental results demonstrate that LNO with Cu-doping can enhance electrochemical performance, and show excellent chromium tolerance working as a promising chromium-tolerant cathode for IT-SOFCs.

IV. Conclusions

In this work, the effect of Cu-doping in the Ruddlesden-Popper-typeoxides LNO and LNCO on the crystal structure, interstitial oxygen formation, electrical conductivity, catalytic activity and chromium tolerance was characterized and evaluated. XRD Rietveld and HT-TEM results together confirm both were identified as the Ruddlesden-Popper-type structures with tetragonal symmetry. LNCO has less interstitial oxygen because the Cu incorporation in the $Ni(Cu)O_6$ octahedron structure restricts the oxygen insertion into the rock salt layer. The electrical conductivity decreases owing to the reduction of the carrier concentration after Cu-doping. The effects on electrode performance using symmetric cells were analyzed, and interface polarization resistance at 800 °C is reduced from 2.20 Ωcm^2 to 0.54 Ωcm^2 after Cu-doping. HT-XRD results indicate both have a relatively high chromium tolerance below 900 °C. The present results demonstrate that LNO with Cu-doping can work as a promising chromium-tolerant cathode.

Acknowledgements

This work was financially supported by the Key Laboratory of Coal-based CO_2 Capture and Geological Storage, Jiangsu Province (No: 6AT158524), the National Natural Science Foundation of China (No. 51602343 and 51402266), the Natural Science Foundation of Jiangsu Province (No. BK20160271), and Postgraduate Research & Practice Innovation Program of Jiangsu Province (No. SJCX17_0528).

References

1 Nakamura, T., Oike, R., Ling, Y., Tamenori, Y., Amezawa, K.: The determining factor for interstitial oxygen formation in Ruddlesden-Popper type La_2NiO^4-based oxides, *Phys. Chem. Chem. Phys.*, **18**, 1564 – 1569, (2016).

2 Li, Z., Haugsrud, R: Effects of surface coatings on the determination of D_{chem} and k_{chem} in $La_2NiO_{4+\delta}$ by conductivity relaxation, *Solid State Ion.*, **206**, 67 – 71, (2012).

3 Ferkhi, M., Ahmed Yahia, H.: Electrochemical and morphological characterizations of $La_{2-x}NiO_{4-\delta}$ (x = 0.01, 0.02, 0.03 and 0.05) as new cathodes materials for IT-SOFC, *Mater. Res. Bull.*, **83**, 268 – 274, (2016).

4 Ling, Y., Wang, F., Okamoto, Y., Nakamura, T., Amezawa, K.: Oxygen nonstoichiometry and thermodynamic explanation of large oxygen-deficient Ruddlesden-Popper oxides $La_xSr_{3-x}Fe_2O_{7-\delta}$, *J. Am. Ceram. Soc.*, **99**, 3792 – 3801, (2016).

5 Sharma, R.K., Burriel, M., Dessemond, L., Martin, V., Bassat, J.M., Djurado, E.: An innovative architectural design to enhance the electrochemical performance of $La_2NiO_{4-\delta}$ cathodes for solid oxide fuel cell applications, *J. Power Sources*, **316**, 17 – 28, (2016).

6 Li, Z., Norby, T., Haugsrud, R.: Synthesis, sintering, transport properties, and surface exchange of $La_2Ni_{0.9}Cu_{0.1}O_{4+\delta}$, *J. Am. Chem. Soc.*, **95**, 2065 – 2073, (2012).

7 Kharton, V.V., Tsipis, E.V., Yaremchenko, A.A., Frade, J.R.: Surface-limited oxygen transport and electrode properties of $La_2Ni_{0.8}Cu_{0.2}O_{4+\delta}$, *Solid State Ion.*, **166**, 327 – 337, (2004).

8 Escudero, M.J., Aguadero, A., Alonso, J.A., Daza, L.: A kinetic study of oxygen reduction reaction on La_2NiO_4 cathodes by means of impedance spectroscopy, *J. Electroanal. Chem.*, **611**, 107 – 116, (2007).

9 Escudero, M.J., Fuerte, A., Daza, L.: $La_2NiO_{4+\delta}$ potential cathode material on $La_{0.9}Sr_{0.1}Ga_{0.8}Mg_{0.2}O_{2.85}$ electrolyte for intermediate temperature solid oxide fuel cell, *J. Power Sources*, **196**, 7245 – 7250, (2011).

10 Nakamura, T., Ling, Y., Amezawa, K.: The effect of interstitial oxygen formation on the crystal lattice deformation in layered perovskite oxides for electrochemical devices, *J. Mater. Chem.*, **A3**, 10471 – 10479, (2015).

11 Vashook, V.V., Tolochko, S.P., Yushkevich, I.I., Makhnach, L.V., Kononyuk, I.F., Altenburg, H., Hauck, J., Ullmann, H.: Oxygen nonstoichiometry and electrical conductivity of the solid solutions $La_{2-x}Sr_xNiO_y$ ($0 \le x \le 0.5$), *Solid State Ion.*, **110**, 245 – 253, (1998).

12 Skinner, S.J., Kilner, J.A.: Oxygen diffusion and surface exchange in $La_{2-x}Sr_xNiO_{4+\delta}$, *Solid State Ion.*, **135**, 709 – 712, (2000).

13 Vashook, V.V., Trofimenko, N.E., Ullmann, H., Makhnach, L.V.: Oxygen nonstoichiometry and some transport properties of $LaSrNiO_{4-\delta}$ nickelate, *Solid State Ion.*, **131**, 329 – 336, (2000).

14 Tucker, M.C., Kurokawa, H., Jacobson, C.P., De Jonghe, L.C., Visco, S.J.: A fundamental study of chromium deposition on solid oxide fuel cell cathode materials, *J. Power Sources*, **160**, 130 – 138, (2006).

15 Jiang, S.P., Chen, X.B.: Chromium deposition and poisoning of cathodes of solid oxide fuel cells – A review, *Int. J. Hydrogen Energy*, **36**, 805 – 821, (2014).

16 Kim, Y.M., Chen, X.B., Jiang, S.P., Bae, J.: Chromium deposition and poisoning at $Ba_{0.5}Sr_{0.5}Co_{0.8}Fe_{0.2}O_{3-\delta}$ cathode of solid oxide fuel cells, *Electrochem. Solid-State Lett.*, **14**, B41 – B45, (2011).

17 Horita, T., Xiong, Y.P., Kishimoto, H., Yamaji, K., Brito, M.E., Yokokawa, H.: Chromium poisoning and degradation at $(La,Sr)MnO_3$ and $(La,Sr)FeO_3$ cathodes for solid oxide fuel cells, *J. Electrochem. Soc.*, **157**, B614 – B620, (2010).

18 Pellegrin, E., Zaanen, J., Lin, H.J., Meigs, G., Chen, C.T., Eisaki, H., Uchida, S.: O1s near-edge X-ray absorption of $La_{2-x}Sr_xNiO_{4+\delta}$: Holes, polarons, and excitons, *Phys. Rev. B*, **53**, 10667 – 10679, (1996).

19 Shen, Y., Zhao, H., Swierczek, K., Du, Z., Xie, Z.: Lattice structure, sintering behavior and electrochemical performance of $La_{1.7}Ca_{0.3}Ni_{1-x}Cu_xO_{4+\delta}$ as cathode material for intermediate temperature solid oxide fuel cell, *J. Power Sources*, **240**, 759 – 765, (2013).

20 Chen, Y., Zhou, W., Ding, D., Liu, M., Ciucci, F., Tade, M., Shao, Z.: Advances in cathode materials for solid oxide fuel Cells: complex oxides without alkaline earth metal elements, *Adv. Energy Mater.*, **18**, 1 – 37, (2015).

21 Ling, Y., Chen, H., Niu, J., Wang, F., Zhao, L., Ou, X., Nakamura, T., Amezawa, K.: Bismuth and indium co-doping strategy for developing stable and efficient barium zirconate-based proton conductors for high-performance H-SOFCs, *J. Eur. Ceram. Soc.*, **36**, 3423 – 3431, (2016).

22 Ling, Y., Lu, X., Niu, J., Chen, H., Ding, Y., Ou, X., Zhao, L.: Antimony doped barium strontium ferrite perovskites as novel cathodes for intermediate-temperature solid oxide fuel cells, *J. Alloy. Compd.*, **666**, 23 – 29, (2016).

23 Choisnet, J., Abadzhieva, N., Stefanov, P., Klissurski, D., Bassat, J.M., Rives, V., Minchev, L.: X-ray photoelectron spectroscopy, temperature-programmed desorption and temperature-programmed reduction study of $LaNiO_3$ and $La_2NiO_{4+\delta}$ catalysts for methanol oxidation, *J. Chem. Soc., Faraday Trans.*, **90**, 1987 – 1991, (1994)

24 Ling, Y., Zhao, L., Liu, X., Lin, B.: Tailoring electrochemical property of layered perovskite cathode by Cu-doping for proton-conducting IT-SOFCs, *Fuel Cells*, **15**, 384 – 389, (2015).

25 Kharton, V.V., Vtsipis, E., Yaremchenko, A.A., Frade, J.R.: Surface-limited oxygen transport and electrode properties of $La_2Ni_{0.8}Cu_{0.2}O_{4-\delta}$, *Solid State Ion.*, **166**, 327 – 337, (2004).

26 Nakamura, T., Yashiro, K., Sato, K., Mizusaki, J.: Electronic state of oxygen nonstoichiometric $La_{2-x}Sr_xNiO_{4+\delta}$ at high temperatures, *Phys. Chem. Chem. Phys.*, **11**, 3055 – 3062, (2009).

27 Boehm, E., Bassat, J.M., Steil, M.C., Dordor, P., Mauvy, F., Grenier, J.C.: Oxygen transport properties of $La_2Ni_{1-x}CuxO_{4+\delta}$ mixed conducting oxides, *Solid State Sci.*, **5**, 973 – 981, (2003).

28 Li, H., Chen, X., Chen, S., Wu, Y., Xie, K.: Composite manganate oxygen electrode enhanced with iron oxide nanocatalyst for high temperature steam electrolysis in a proton-conducting solid oxide electrolyzer, *Int. J. Hydrogen Energy*, **40**, 7920 – 7931, (2015).

29 Ralph, J.M., Schoeler, A.C., Krumpelt, M.: Materials for lower temperature solid oxide fuel cells, *J. Mater. Sci.*, **36**, 1161 – 1172, (2001).

30 Chen, D., Huang, C., Ran, R., Park, H., Kwak, C., Shao, Z.: New $Ba_{0.5}Sr_{0.5}Co_{0.8}Fe_{0.2}O_{3-\delta}$ $+Co_3O_4$ composite electrode for IT-SOFCs with improved electrical conductivity and catalytic activity, *Electrochem. Commun.*, **13**, 197 – 199, (2011).

31 Aguadero, A., Alonso, J.A., Escudero, M.J., Daza, L.: Evaluation of the $La_2Ni_{1-x}Cu_xO_{4+\delta}$ system as SOFC cathode material with 8YSZ and LSGM as electrolytes, *Solid State Ion.,* **179**, 393 – 400, (2008).

32 Nakamura, T., Yashiro, K., Sato, K., Mizusaki, J.: Thermodynamic quantities and defect equilibrium in $La_{2-x}Sr_xNiO_{4+\delta}$, *J. Solid State Chem.*, **182**, 1121 – 1128, (2009).

33 Makhnach, L.V., Pankov, V.V., Strobel, P.: High-temperature oxygen non-stoichiometry, conductivity and structure in strontium-rich nickelates $La_{2-x}Sr_xNiO_{4-\delta}$ (x = 1 and 1.4), *Mater. Chem. Phys.*, **111**, 125 – 130, (2008).

34 Ling, Y., Wang, F., Budiman, R. Nakamura, T., Amezawa, K.: Oxygen nonstoichiometry, the defect equilibrium model and thermodynamic quantities of the ruddlesden-popper oxide $Sr_3Fe_2O_{7-\delta}$, *Phys. Chem. Chem. Phys.*, **17**, 7489 – 7497, (2015)

35 Ling, Y., Guo, T., Zhang, X., Budiman, R., Fujimaki, Y., Nakamura, T., Lin, B., Kawada, T., Amezawa, K.: Evaluation of electrical conductivity and oxygen diffusivity of the typical ruddlesden-popper oxide $Sr_3Fe_2O_{7-\delta}$, Ceram. Int., **48**, 16264 – 16269, (2017).